# Inductively Coupled 180-nm CMOS Charger with Adjustable Energy-Investment Capability

Orlando Lazaro, *Graduate Student Member, IEEE,* Gabriel A. Rincón-Mora, *Fellow, IEEE*

***Abstract*—Although wireless microsensors can add performance-enhancing and energy-saving intelligence to factories, hospitals, and others, their tiny on-board sources exhaust quickly. Luckily, coupling power inductively can both energize system components and recharge a battery. Miniaturized receiver coils, however, capture a small fraction of the magnetic energy available, so coupling factors ($k_C$) and, as a result, power-conversion efficiencies are low. In other words, damping the magnetic source so it outputs maximum power is difficult. Investing energy into the coil increases its ability to draw power, but only when optimized. Since state-of-the-art systems can only recycle harvested energy, they are optimal only at one $k_C$ value. The inductively coupled 180-nm CMOS charger prototyped, measured, and presented here invests programmable amounts of battery energy into the pickup coil to generate 8 – 390 µW when $k_C$ is 0.009 – 0.076 and raise output power by 132% and 24% at $k_C$'s of 0.020 and 0.076, respectively.**

***Index Terms*—Inductively coupled power, contactless battery charger, wireless power, energy investment, electrical damping.**

## I. Inductively Powered Microsystems

Emerging wireless microsystems include sensors, processors, memory, transmitters, and other components that sensor networks [1] and biomedical implants [2] use to improve performance and save energy. Collecting, processing, storing, and transmitting data over time, however, typically requires more power and energy [3] than tiny lithium-ion batteries and super capacitors can supply [4]. As a result, the functionality of a node is normally low and lifetime is short.

Coupling power inductively into the system, as Fig. 1 shows, can both increase functionality and extend operational life. In fact, by energizing functional blocks directly (via a power conditioner) [5] and recharging an onboard battery $C_{BAT}$ [6], the system can save battery energy and operate later, on demand between recharge cycles. The problem is only a small fraction of the magnetic flux that the transmitting source generates penetrates the system's tiny pickup coil $L_S$, which means that, for a given coil separation $d_C$, coupling factor $k_C$ and induced electromotive-force voltage $v_{EMF.S}$ are low [7].

Fortunately, raising the coil's current, as Section II describes, further dampens the transmitting source, so $L_S$ draws more power. Resonant-based bridges [8] invest energy for this purpose, except conversion efficiency is sensitive to frequency and investment levels cannot adjust to account for investment losses or over-damping limits. Sections III, IV, and V therefore present, validate, and evaluate an inductively coupled CMOS charger that both, is less sensitive to frequency and invests an adjustable amount of energy. The novelty and focus here is how to invest optimal amounts of battery energy to boost output power for any coupling factor $k_C$ because state-of-the-art resonant systems can only re-cycle harvested energy to draw maximum power at a particular $k_C$.

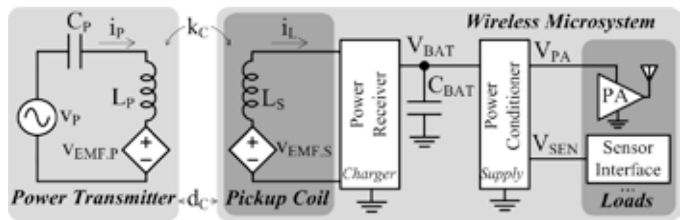


**Fig. 1.** Inductively (i.e., wirelessly) powered microsystem.

## II. Investing Energy in the Pickup Coil

<u>Sourced EMF Voltage</u>: Transmitting ac voltage $v_P$ in Fig. 1 is the ultimate source of power for the system. For that, $v_P$ drives the tuned resonant tank that $C_P$ and $L_P$ implement at operational frequency $f_O$. Some of the magnetic flux that $L_P$'s current $i_P$ generates penetrates $L_S$ to induce an electromotive-force voltage $v_{EMF.S}$ that increases with coupling factor $k_C$, $L_P$, $L_S$, and changes in $v_P$, or by translation, $di_P/dt$:

$$v_{EMF.S} = k_C\sqrt{L_P L_S}\left(\frac{di_P}{dt}\right). \quad (1)$$

Unfortunately, because coil distance $d_C$ reduces the intensity of the magnetic field at $L_S$ and a small pickup coil captures only a fraction of the magnetic flux present, $k_C$ is considerably low, so $v_{EMF.S}$ in microsystems is typically in millivolts.

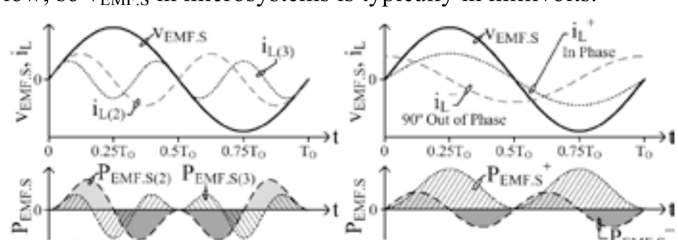


**Fig. 2.** Pickup coil's EMF voltage, harmonics of current, and power.

<u>Power Generated</u>: A positive voltage, like a battery, sources power when current flows out: when current is also positive. Similarly, $v_{EMF.S}$ sources power $P_{EMF.S}$ when $v_{EMF.S}$ and its current $i_L$ are both positive or both negative. This is why $i_L$'s second harmonic $i_{L(2)}$ in Fig. 2a and currents out of phase by $90^O$ $i_L^-$ in Fig. 2b source power between 0 and $0.25T_O$. Conversely, $v_{EMF.S}$ *consumes* power when $v_{EMF.S}$'s and $i_L$'s polarities oppose, so $i_{L(2)}$ and $i_L^-$ between $0.25T_O$ and $0.5T_O$

Manuscript received October 19, 2012. Texas Instruments funded this research.

The authors are with the Georgia Tech Analog, Power, and Energy IC Research Laboratory in the School of Electrical and Computer Engineering at the Georgia Institute of Technology, Atlanta, GA 30332-0250 U.S.A. (E-mail: Orlando.Lazaro@ece.gatech.edu; Rincon-Mora@gatech.edu).

lose energy. As a result, given the symmetry of the signals, $i_L^-$ and $i_{L(2)}$, like all other even harmonics, generate as much power as they dissipate across every half cycle. In other words, $90^O$ out-of-phase currents and even-order harmonics of $i_L$ do not produce power.

Although third-order harmonic $i_{L(3)}$ in Fig. 2a generates more power than it dissipates across the first half of period $T_O$, it consumes more than it produces across the latter half to *just* cancel earlier gains. As a result, third- and other odd-order harmonics do not produce power. In fact, only in-phase components of $i_L$ draw power from $v_{EMF.S}$ [9]:

$$P_{EMF.S} = \frac{1}{T_O}\int_0^{T_O} v_{EMF.S}\, i_L^+ dt . \quad (2)$$

However, since $v_{EMF.S}$ is in mV's and mV's across $L_S$ induce low $i_L^+$ currents, $P_{EMF.S}$ in unassisted microsystems is low.

Value of Investment: One way of increasing $P_{EMF.S}$ is by enlisting external assistance to raise in-phase current $i_L^+$. That is to say, investing energy in the pickup coil increases $P_{EMF.S}$, but only if the system recovers the investment, transfer losses do not negate the gains, and the system does not over-damp the transmitter. The idea is the 2.7 – 4.2 V that a lithium-ion battery outputs, for example, can quickly raise $i_L^+$ to a substantially higher level $I_{INV}$ than $v_{EMF.S}$ can with $I_{EMF}$. As a result, the quadratic rise in $L_S$'s energy $E_{LS}$ outpaces the initial investment of $0.5L_SI_{INV}^2$ to generate a gain that is greater than what $v_{EMF.S}$'s $I_{EMF}$ alone can produce with $0.5L_SI_{EMF}^2$ [8]:

$$\begin{aligned} E_{LS} &= 0.5L_S i_{L(PK)}^2 = 0.5L_S\left(I_{INV}+I_{EMF}\right)^2 \\ &= 0.5L_S I_{INV}^2 + 0.5L_S I_{EMF}^2 + L_S I_{INV} I_{EMF} . \end{aligned} \quad (3)$$

Since $k_C$ is low in microsystems, extracting power hardly damps the transmitting source, so higher investments draw more power from $v_P$. This trend only continues, however, if the power losses that result from investing $0.5L_SI_{INV}^2$ do not exceed the incremental gain of $L_SI_{INV}I_{EMF}$. This presents a limit because Ohmic $i_{RMS}^2R$ losses in $L_S$'s conduction path rise quadratically with increasing investment currents, so quadratic losses outpace linear gains in $L_SI_{INV}I_{EMF}$ to a point where raising the investment does not help.

When the pickup coil is sufficiently larger and/or closer to the transmitting source, the coupling factor can be so high that investing more energy over-damps $v_P$ [10–12] before investment losses negate incremental gains. In other words, over-damping, which reduces $i_P$ and therefore $v_{EMF.S}$, poses another investment limit. The two limits imply that an optimal investment current $I_{INV}^*$ delivers maximum power. For this, the system must adjust and both supply and sink investment current because in-phase current changes polarity with $v_{EMF.S}$. Notice the investment helps draw more energy from $v_{EMF.S}$ as described only when $i_L$ remains in phase with $v_{EMF.S}$.

## III. Investment-assisted Inductively Coupled Charger

Operation: The circuit in Fig. 3 draws battery power from $C_{BAT}$ to invest energy in pickup coil $L_S$. For this, $S_D^-$ and $S_N^+$ first connect to energize $L_S$ with $v_{EMF.S}$ when $v_{EMF.S}$ is positive and $V_{BAT}$ through positive investment time $\tau_{INV}^+$. With $V_{BAT}$'s higher voltage across $L_S$, $L_S$'s $i_L$ rises quickly to $I_{INV}^+$, as Fig. 4 shows. Through this time, $v_{EMF.S}$ and $V_{BAT}$ deposit energy into $L_S$. Past $\tau_{INV}^+$, $S_D^-$ opens and $S_N^-$ closes to continue energizing $L_S$ from $v_{EMF.S}$ through the remainder of $v_{EMF.S}$'s positive half cycle, as the measured waveforms of Fig. 4 show across $\tau_E^+$.

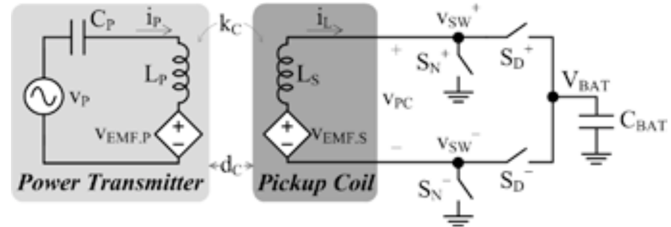


**Fig. 3.** Investment-assisted inductively coupled charger.

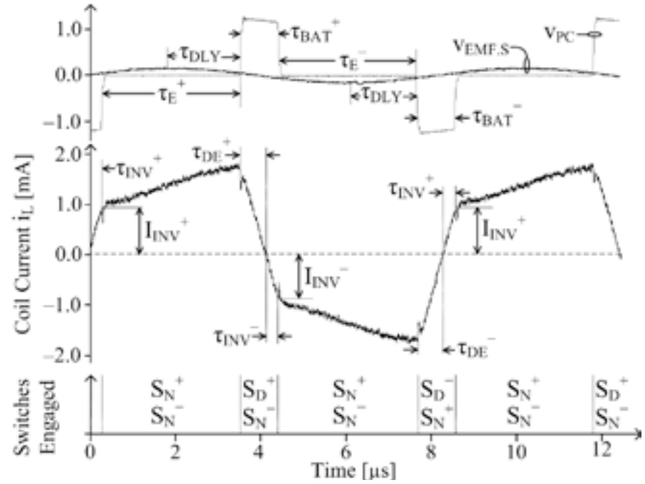


**Fig. 4.** Extrapolated $v_{EMF.S}$ from measured coil voltage $v_{PC}$ and current $i_L$.

At the end of $v_{EMF.S}$'s positive half cycle: at the end of $\tau_E^+$, $S_N^+$ opens and $S_D^+$ closes to deplete $L_S$ into $C_{BAT}$ and, after that, draw investment current from $C_{BAT}$. $S_D^+$ basically reverses $V_{BAT}$'s polarity across $L_S$ to decrease $i_L$ quickly across de-energizing and negative investment times $\tau_{DE}^+$ and $\tau_{INV}^-$ to zero and past zero to $-I_{INV}^-$. $S_D^+$ then opens and $S_N^+$ closes to further energize $L_S$ from $v_{EMF.S}$ across $v_{EMF.S}$'s negative half cycle until $i_L$ peaks in the negative direction at the end of $\tau_E^-$. As at the end of $\tau_E^+$, $S_N^-$ opens and $S_D^-$ closes at the end of $\tau_E^-$ to drain $L_S$ into $C_{BAT}$ and invest $C_{BAT}$ charge into $L_S$ across de-energizing and positive investment times $\tau_{DE}^-$ and $\tau_{INV}^+$. Table I summarizes the states of the switches, their duration, and the coil voltages they establish across $T_O$.

**TABLE I**: State Diagram

| State of $v_{EMF.S}$ | Duration | $v_{PC}$ | $S_N^+$ | $S_D^+$ | $S_N^-$ | $S_D^-$ |
|---|---|---|---|---|---|---|
| –/+ Transition | $\tau_{BAT}^- = \tau_{DE}^- + \tau_{INV}^+$ | $-V_{BAT}$ | On | Off | Off | On |
| + | $\tau_E^+$ | 0 | On | Off | On | Off |
| +/– Transition | $\tau_{BAT}^+ = \tau_{DE}^+ + \tau_{INV}^-$ | $+V_{BAT}$ | Off | On | On | Off |
| – | $\tau_E^-$ | 0 | On | Off | On | Off |

Output Power: $C_{BAT}$ receives energy from $L_S$ across $v_{EMF.S}$'s positive and negative cycles' de-energizing times $\tau_{DE}^+$ and $\tau_{DE}^-$ and invests charge across positive and negative investment times $\tau_{INV}^+$ and $\tau_{INV}^-$. As a result, assuming $L_S$ transfers energy losslessly and $I_{INV}^+$ mirrors $I_{INV}^-$, $C_{BAT}$'s net energy gain per cycle is

$$E_{BAT} \approx 2\left(0.5L_S i_{L(PK)}^2\right) - 2\left(0.5L_S I_{INV}^2\right) = L_S\left(I_{EMF}^2 + 2I_{EMF}I_{INV}\right), \quad (4)$$

where $i_L$'s peak $i_{L(PK)}$ is $I_{INV}$ plus $v_{EMF.S}$'s contribution $I_{EMF}$ across each half cycle, which is

$$I_{EMF} = \int_0^{\tau_E} \frac{v_{EMF.S(PK)} \sin(2\pi f_O t)}{L_S} dt . \quad (5)$$

In other words, $v_{EMF.S}$ sources

$$P_{EMF.S} \approx \frac{L_S\left(I_{EMF}{}^2 + 2I_{EMF}I_{INV}\right)}{T_O} = L_S\left(I_{EMF}{}^2 + 2I_{EMF}I_{INV}\right)f_O . \quad (6)$$

$L_S$'s series resistance $R_S$ and $S_N^+$, $S_N^-$, $S_D^+$, $S_D^-$, and the controller circuit (which Fig. 3 does not show), however, consume energy, so the battery receives less power:

$$P_{BAT} = P_{EMF.S} - P_{LOSS} . \quad (7)$$

Note the analysis assumes $i_L$ and $v_{EMF.S}$ are in phase, so the controller should start draining $L_S$ just before $v_{EMF.S}$ reaches zero in Fig. 4 to ensure $i_L$ and $v_{EMF.S}$ have the same polarity. Otherwise, with opposite polarities, $v_{EMF.S}$ extracts energy from $L_S$, which is effectively an additional loss in $P_{LOSS}$.

## IV. Prototyped Inductively Coupled System

Fig. 5 illustrates the investment-assisted inductively coupled charger fabricated, prototyped, and measured. The 350 × 700-μm² 180-nm CMOS IC houses the power receiver, except for the 400-μH 3.5 × 2.6 × 11.7-mm³ pickup coil, the 100-nF 0.5 × 1.0 × 0.4-mm³ battery capacitor $C_{BAT}$, synchronizer, and a bias resistor, the latter of two of which are off chip for testing purposes. Here, CMOS transistors $M_N^+$, $M_N^-$, $M_P^+$, and $M_P^-$ implement switches $S_N^+$, $S_N^-$, $S_D^+$, and $S_D^-$ from Fig. 3. So, while keeping transmission strength constant, variations in coil distance $d_C$ changed coupling factor $k_C$ to test the impact of investments on $P_{EMF.S}$ across $v_{EMF.S}$ levels. The system outputs power when the coils are up to 11.35 mm apart.

Control: The synchronizer prompts the system to draw energy from $L_S$ when $v_{EMF.S}$ transitions between half cycles, as Fig. 4 shows. So, when $S_{SYN}$ trips low, at the end of $\tau_E^+$, $M_N^+$ opens and $L_S$'s current $i_L$ raises $v_{SW}^+$ to the point comparator $CP_D^+$ closes $M_P^+$. After $L_S$ depletes into $C_{BAT}$, $CP_D^+$'s intentional input-referred offset $V_{OS}^+$ keeps $M_P^+$ closed to let $C_{BAT}$ energize $L_S$ in the negative direction. This continues until $i_L$, which now flows out of $C_{BAT}$, impresses a voltage across $M_P^+$ that is large enough to overcome $V_{OS}^+$. At this point, which marks the end of $\tau_{INV}^-$, $CP_D^+$ shuts $M_P^+$ and closes $M_N^+$ to allow $v_{EMF.S}$ energize $L_S$ across the negative half cycle.

$S_{SYN}$ similarly opens $M_N^-$ when $S_{SYN}$ trips high at the end of $\tau_E^-$ to steer $i_L$ into $v_{SW}^-$, which raises $v_{SW}^-$ until $CP_D^-$ engages $M_P^-$ and drains $L_S$ into $C_{BAT}$. $CP_D^-$ keeps $M_P^-$ closed until after $i_L$ reverses and establishes a voltage across $M_P^-$ that is sufficiently high to overcome $CP_D^-$'s offset $V_{OS}^-$, at the end of $\tau_{INV}^+$. $v_{EMF.S}$ continues to energize $L_S$ after that across $\tau_E^+$ until $S_{SYN}$ restarts another cycle.

The difference between this system and [13] is this one invests battery energy into $L_S$, which [13] cannot do. Here, after harvesting charge into $C_{BAT}$, $S_D^+$ and $S_D^-$ draw energy from $C_{BAT}$ to invest into $L_S$. Since $C_{BAT}$'s current $i_{BAT}$ across $M_P^+$ and $M_P^-$ trip $CP_D^+$ and $CP_D^-$ at the end of $\tau_{INV}^-$ and $\tau_{INV}^+$, $V_{OS}^+$ and $V_{OS}^-$ together with $M_P^+$ and $M_P^-$'s triode resistances (i.e., $R_P$) limit $C_{BAT}$'s half-cycle investment in $L_S$ to

$$I_{INV} = \frac{V_{OS}}{R_P} . \quad (8)$$

Power Losses: As already mentioned, resistances, switches, and the controller consume energy that would otherwise reach $C_{BAT}$. $i_L$, for example, dissipates Ohmic power $P_C$ in $L_S$'s $R_S$ and $M_N^+$ and $M_N^-$ across $L_S$'s energizing times $\tau_E^+$ and $\tau_E^-$. Similarly, $R_S$ and $M_N^-$ and $M_P^+$ (and $M_N^+$ and $M_P^-$) consume power across $L_S$'s de-energizing and investment times $\tau_{DE}^+$ and $\tau_{INV}^-$ (and $\tau_{DE}^-$ and $\tau_{INV}^+$). As a result, $P_C$ combines to

$$P_C = (2R_N + R_S)i_{L.E(RMS)}{}^2 + (R_N + R_P + R_S)i_{L.BAT(RMS)}{}^2 , \quad (9)$$

where $R_N$ and $R_P$ are n- and p-type MOS triode resistances.

The battery also loses energy $E_G$ each time the drivers charge MOS gate capacitors to $V_{BAT}$. As a result, combined gate capacitance $C_G$ draws gate-drive power $P_G$ from $C_{BAT}$:

$$P_G = \frac{E_G}{T_O} = (Q_C V_{BAT}) f_O = C_G V_{BAT}{}^2 f_O . \quad (10)$$

$CP_D^+$ and $CP_D^-$ also draw quiescent battery power $P_Q$, except the logic in Fig. 5 enables them at the end of $\tau_E^+$ and $\tau_E^-$ and disables them at the end of $\tau_{INV}^-$ and $\tau_{INV}^+$, so they lose

$$P_Q = 2P_{CP} = 2(I_{CP}V_{BAT})\left(\frac{\tau_{DE} + \tau_{INV}}{T_O}\right) . \quad (11)$$

Investment Limits: Of the three loss components in $P_{LOSS}$:

$$P_{LOSS} = P_C + P_G + P_Q , \quad (12)$$

conduction losses $P_C$ and quiescent losses $P_Q$ increase with investment level $I_{INV}$. For example, because $L_S$ requires more time to drain and energize to a higher current, raising $I_{INV}$ extends de-energizing and investment times $\tau_{DE}$ and $\tau_{INV}$. A higher $I_{INV}$ also means $i_{L(RMS)}$ is higher, which means $P_C$ rises quadratically with $I_{INV}$. This is significant because, since sourced power $P_{EMF.S}$ rises linearly with $i_L$, elevating $I_{INV}$ via $V_{OS}$ raises $P_{BAT}$, but only until losses negate incremental gains, which means $P_{BAT}$ is highest at an optimal investment level.

Before reaching this limit, however, raising $P_{EMF.S}$ can also

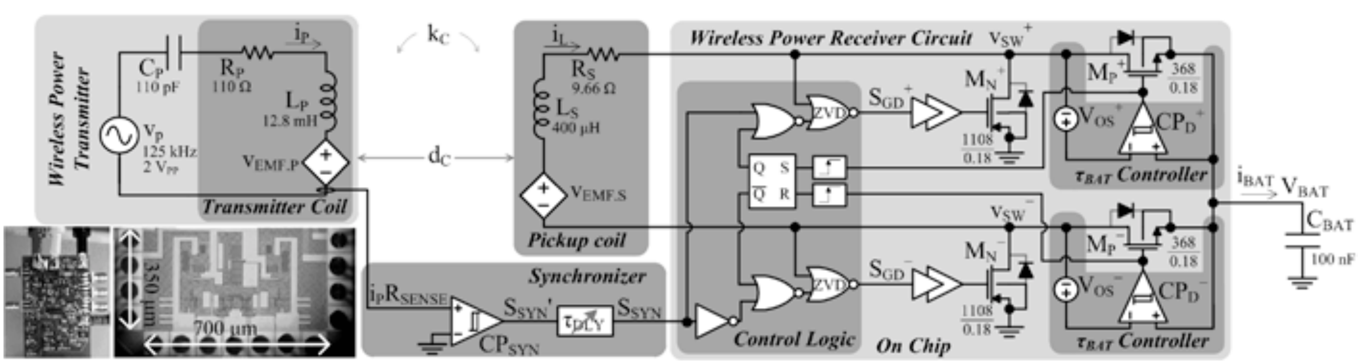


**Fig. 5.** Prototyped inductively coupled 180-nm CMOS charger with adjustable energy investment (transistor dimensions are in μm).

over-damp the transmitting source. This results because drawing power from $v_{EMF.S}$ is equivalent to loading $v_{EMF.S}$, whose effect on the transmitter is to load it. In Fig. 6, for example, since $L_S$'s $i_L$ integrates $v_{EMF.S}$'s sinusoid, $L_S$ models $90^O$ out-of-phase components of $i_L$ and resistor $R_{EQ}$ models in-phase components, which is why $R_{EQ}$ is $v_{EMF.S(PK)}/i_L^+$. Such a load reflects back on the transmitter as the series combination of inductor $L_{S.P}$ and resistor $R_{EQ.P}$. As a result, $v_P$ sources maximum power when its equivalent load of $L_{S.P}$ and $R_{EQ.P}$ matches $v_P$'s source impedance of $R_P$, $L_P$, and $C_P$. In other words, $P_{EMF.S}$ is highest at an optimal investment level.

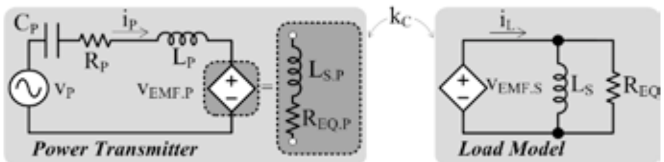


**Fig. 6.** Power receiver's load model and its reflection on the transmitter.

Another possibility is that the system maxes $i_L$ before losses overwhelm incremental gains and $P_{EMF.S}$ over-damps $v_P$. Reaching this $i_{L(MAX)}$ limit happens when $\tau_{DE}$ and $\tau_{INV}$ extend through $v_{EMF.S}$'s entire half cycle of $0.5T_O$, as Fig. 7 shows:

$$i_{L(MAX)} = \int_{0}^{\tau_{DE}+\tau_{INV}} \left(\frac{V_{BAT} + v_{EMF.S}}{L_S}\right) dt = \int_{0.25T_O}^{0.75T_O} \left(\frac{V_{BAT} + v_{EMF.S}}{L_S}\right) dt . \quad (13)$$

In other words, the system has no more than half a cycle to drain and energize $L_S$ to and from $i_{L(MAX)}^+$ and $i_{L(MAX)}^-$. Here, a strong transmitting source $v_P$ and/or a high coupling factor $k_C$, both of which raise $v_{EMF.S}$, and/or a large $V_{BAT}$ can max $i_L$.

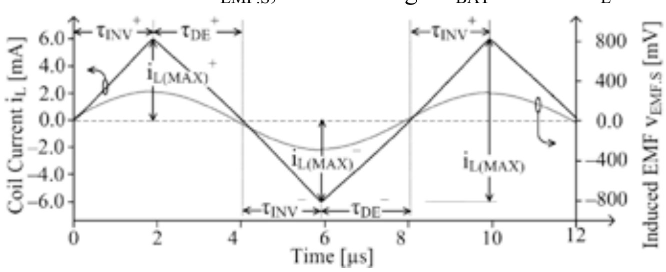


**Fig. 7.** System maxes pickup coil's $i_L$ when $\tau_{DE}$ and $\tau_{INV}$ extend to $0.5T_O$.

Synchronizer: As mentioned in Section II, matching $i_L$'s polarity to that of $v_{EMF.S}$ keeps $v_{EMF.S}$ from consuming power. For this, the synchronizer prompts the system to drain $L_S$ just before $v_{EMF.S}$ transitions between half cycles and invest battery energy into $L_S$ after the transition. Since transmitter current $i_P$ dictates how $v_{EMF.S}$ behaves, timing the system to $i_P$ is possible. Comparator $CP_{SYN}$ in Fig. 5, for example, trips when $i_P$ crosses zero, which is when $v_{EMF.S}$ peaks in Fig. 4, and manually tunable delay block $\tau_{DLY}$ waits until $v_{EMF.S}$ is close enough to the next half cycle to start draining $L_S$ into $C_{BAT}$.

Unfortunately, sensing $i_P$ is not always plausible. Disconnecting $L_S$ across one or two periods to sense and program $v_{EMF.S}$'s transition points for subsequent cycles is another way to time the system. The transmitter can also send this information across $L_P$–$L_S$'s inductive link. Note $CP_{SYN}$–$\tau_{DLY}$ in Fig. 5 is only an example used to assess the efficacy of investing battery energy, which is the focus of this work.

## V. Measured Performance

Output Power: Fig. 8 shows higher $I_{INV}$ values draw more $P_{EMF.S}$ from $v_{EMF.S}$ for low coupling factors. The figure also demonstrates that raising $P_{EMF.S}$ hardly affects $v_{EMF.S}$, so damping effects on the transmitting source are minimal in this coupling regime. Battery power $P_{BAT}$, however, maxes at 82 µW with an optimal investment of 1.9 mA, when losses $P_{LOSS}$ offset incremental gains. Notice conduction losses $P_C$ rise quickly with $I_{INV}$ to dominate $P_{LOSS}$ and limit $P_{BAT}$. Also note $P_{BAT(MAX)}$ is nearly half of $P_{EMF.S}$ at 1.9 mA, which means source and load impedances in the receiver nearly match to yield maximum output power [10, 12]. However, because $P_{LOSS}$ also includes gate-drive and quiescent losses $P_G$ and $P_Q$, $P_{BAT}$ is slightly below its theoretical maximum.

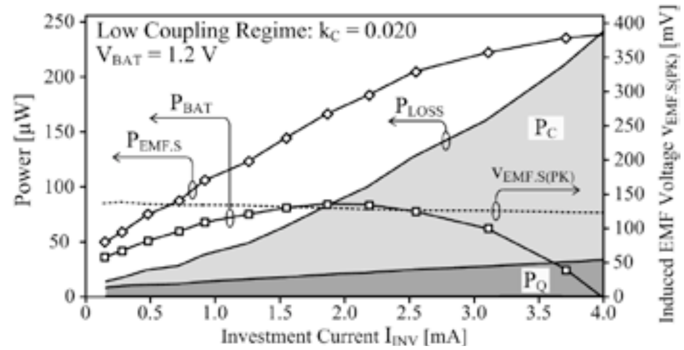


**Fig. 8.** Measured power and extrapolated $v_{EMF.S}$ across investment levels when coupling factor is low at 0.020.

With a higher coupling factor $k_C$, elevating $I_{INV}$ reduces $v_{EMF.S}$ in Fig. 9, so the transmitter suffers more damping effects in this coupling regime. $P_{EMF.S}$ therefore maxes at 506 µW with 2.5 mA. Because $P_{LOSS}$ still consumes some of $P_{EMF.S}$, however, $P_{BAT}$ maxes at 392 µW with a different investment level of 1.4 mA. Note $P_{BAT}$ is higher than in the low coupling case because $v_{EMF.S}$ generates more power with a higher $k_C$.

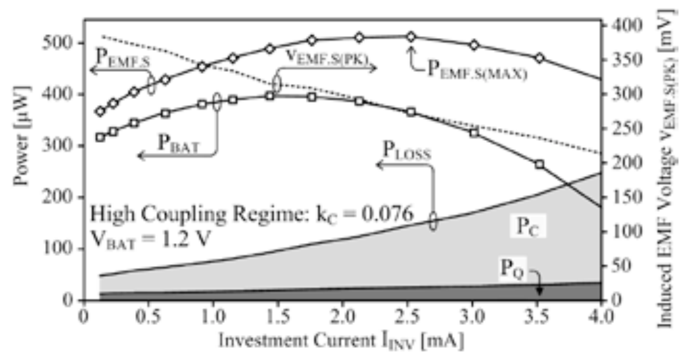


**Fig. 9.** Measured power and extrapolated $v_{EMF.S}$ across investment levels when coupling factor is high at 0.076.

System Efficiency: While wall outlets, for example, can often afford to flood transmitters with power, batteries in emerging applications cannot. In these latter cases, conserving energy across the system may be more important than supplying maximum power. Therefore, to maximize system efficiency $\eta_{SYS}$, designers must negotiate tradeoffs between transmitter and receiver efficiencies $\eta_T$ and $\eta_R$, respectively:

$$\eta_{SYS} = \eta_T \eta_R = \left(\frac{P_{EMF.S}}{P_P}\right)\left(\frac{P_{BAT}}{P_{EMF.S}}\right), \quad (14)$$

where $\eta_T$ is the fraction of $v_P$'s power that $v_{EMF.S}$ captures in $P_{EMF.S}$ and $\eta_R$ is the portion of $P_{EMF.S}$ $C_{BAT}$ receives as $P_{BAT}$.

In this context, because quadratic receiver losses outgrow linear increases in $P_{EMF.S}$ in response to higher investments, receiver efficiencies $\eta_R$ in Figs. 10 and 11 decrease with $I_{INV}$. Since higher investments damp the transmitting source further, $v_P$'s current $i_P$ also falls with $I_{INV}$. As such, because source power $P_P$ drops linearly with $i_P$ and conduction losses $P_{C(T)}$ in the transmitter fall quadratically with $i_P$, savings in $P_{C(T)}$ outpace losses in $P_P$ with higher $I_{INV}$ levels, so transmission efficiency $\eta_T$ increases with $I_{INV}$. System efficiency $\eta_{SYS}$, as a result, peaks when power losses in the receiver balance savings in the transmitter at 1.9 and 2.5 mA in the low and high coupling regimes, respectively. Note $\eta_{SYS}$ in Fig. 11 maxes at a higher point than $P_{BAT}$ in Fig. 9 because, although losses in the receiver are severe enough to limit $P_{BAT}$ at 1.4 mA, savings in the transmitter are greater up to 2.5 mA.

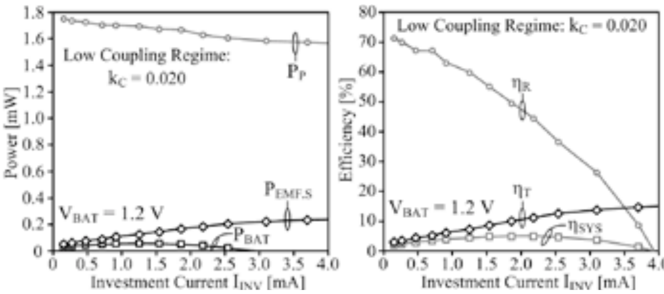


**Fig. 10.** Measured efficiencies and power across investment levels when coupling factor is low at 0.020.

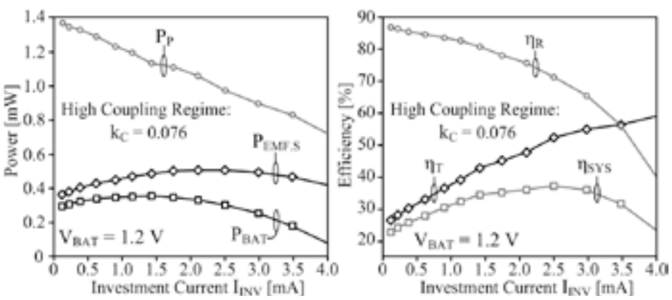


**Fig. 11.** Measured efficiencies and power across investment levels when coupling factor is high at 0.076.

Maximum Output Power: The driving objective for this particular prototype is maximum output power $P_{BAT}$. Here, as Fig. 12 shows, optimal investment $I_{INV}^*$ maxes and remains nearly the same at 2.2 mA for coupling factors $k_C$ ranging from 0.035 to 0.055. This is because losses overwhelm damping effects below 0.035 and *vice versa* above 0.055. In other words, raising $k_C$ to 0.035 means $v_{EMF.S}$ sources more power, so the system can afford to lose more power with a higher $I_{INV}$. Increasing $k_C$ above 0.055, however, reduces $P_{EMF.S}$, so the system cannot afford to lose more power with a higher $I_{INV}$.

## VI. CONCLUSIONS

Measured results show that the inductively coupled 180-nm CMOS charger prototyped here invests battery energy into its pickup coil to generate 8 – 390 μW when coupling factor is 0.009 – 0.076, raising output power by 132% at 0.020 and 24% at 0.076. Investing power, however, increases losses in the receiver and damping effects in the transmitter, which means over-investing is possible. Still, unlike in the state of the art, the investment level is adjustable and drawn from the battery, so the system can output the highest power possible at any coupling factor. This is significant because tiny coils in microsystems capture a small fraction of the magnetic flux present and the batteries of transmitting sources have finite energy. Future wireless microsystems that track the charger's maximum power point and find the optimal investment time across coil separation and orientation and transmission strength can extend their life and functionality this way.

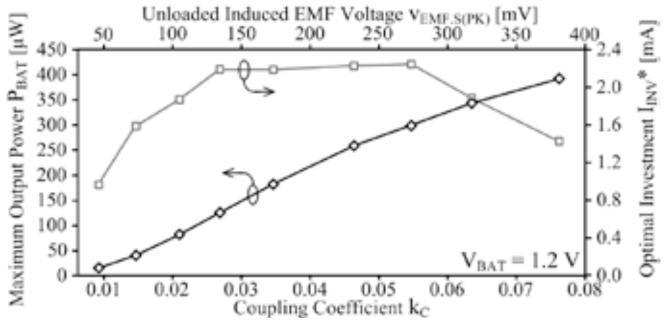


**Fig. 12.** Measured maximum output power across coupling factors.

## REFERENCES


[1] B.W. Cook, S. Lanzisera, and K.S.J. Pister, "SoC issues for RF smart dust," *Proc. IEEE*, vol. 94, no. 6, pp. 1177−1196, Jun. 2006.

[2] G. Chen, H. Ghaed, R. Haque, M. Wieckowski, Y. Kim, G. Kim, D. Fick, D. Kim, M. Seok, K. Wise, D. Blaauw, and D. Sylvester, "A cubic-millimeter energy-autonomous wireless intraocular pressure monitor," in *Int. Solid-State Circuits Conf. (ISSCC) Dig. Tech. Papers*, Feb. 2011, pp. 310−312.

[3] G. Chen, S. Hanson, D. Blaauw, and D. Sylvester, "Circuit design advances for wireless sensing applications," *Proc. IEEE*, vol. 98, no. 11 pp. 1808-1827, Nov. 2010.

[4] D. Linden and T.B. Reddy, "Handbook of Batteries, 4th ed. New York: McGraw-Hill, 2010.

[5] M.W. Baker and R. Sarpeshkar, "Feedback analysis and design of RF links for low-power bionic systems," *IEEE Trans. Biomed. Circuits Syst.*, vol. 1 no. 1, pp. 28−38, Mar. 2007.

[6] P. Li and R. Bashirullah, "A wireless power interface for rechargeable battery operated medical implants," *IEEE Trans. Circuits Syst. II, Exp. Briefs,* vol. 54, no. 10, pp.912−916, Oct. 2007.

[7] F.W. Grover, *Inductance Calculations: Working Formulas and Tables.* New York: D. Van Nostrand Co., 1946.

[8] R.D. Prabha, D. Kwon, O. Lazaro, K.D. Peterson, and G.A. Rincón-Mora, "Increasing electrical damping in energy-harnessing transducers," *IEEE Trans. Circuits Syst. II, Exp. Briefs,* vol. 58, no. 12, pp. 787−791, Dec. 2011.

[9] R.W. Erickson and D. Maksimović, "Power and Harmonics in Nonsinusoidal Systems" in *Fundamentals of Power Electronics*, 2nd ed. New York: Springer, 2001, ch. 16, pp. 589−607.

[10] B. Lenaerts and R. Puers, *Omnidirectional Inductive Powering for Biomedical Implants.* Dordrecht: Springer, 2009.

[11] H.L. Li, A.P. Hu, G.A. Covic, and C.S. Tang, "Optimal coupling condition of IPT system for achieving maximum power transfer," *IET Electron. Lett.,* vol. 45, no. 1, pp. 76−77, Jan. 2009.

[12] M. Zargham and P.G. Gulak, "Maximum achievable efficiency in near-field coupled power-transfer systems", *IEEE Trans. Biomed. Circuits Syst.,* vol. 6, no. 3, pp. 228−245, Jun. 2012.

[13] O. Lazaro and G.A. Rincón-Mora, "Minimizing MOSFET Power Losses in Near-field Electromagnetic Energy-harnessing ICs," in *Int. SoC Design Conf. (ISOCC)*, Jeju, Korea, Nov. 2011, pp. 377−380.